Mechanical Properties and Deformation Mechanisms in High Thermal Resistant Poly(acrylonitrile–butadiene–styrene) Under Static Tension and Izod Impact

P.-Y. B. JAR,[1] D. C. CREAGH,[2] K. KONISHI,[3] T. SHINMURA[3]

[1] Department of Mechanical Engineering, University of Alberta, Edmonton T6G 2G8, Canada

[2] Division of Management and Technology, University of Canberra, Canberra, ACT 2601, Australia

[3] Research & Development Department, Chiba Plant, DENKA, Chiba 290, Japan

Received 23 February 2001; Accepted 16 August 2001

ABSTRACT: Deformation mechanisms in a high thermal resistant poly(acrylonitrile–butadiene–styrene) (ABS) were investigated using transmission electron microscopy (TEM) and small-angle X-ray scattering (SAXS). The work followed our previous study, in which TEM was used for the craze observation and SAXS for the shear yielding, to evaluate the relationship between the mechanical properties and the deformation mechanisms of the ABS under static tension and Izod impact. The current results support our previous conclusion that the combination of TEM and SAXS enables us to identify the deformation mechanisms in the ABS, and provide new evidence for the coexistence of crazing and shear yielding. The SAXS patterns suggest that shear yielding occurred in the ABS, even under the impact loading. We concluded from the study that the occurrence of shear yielding had a major effect on the toughness enhancement of the ABS. © 2002 Wiley Periodicals, Inc. J Appl Polym Sci 85: 17–24, 2002

Key words: transmission electron microscopy; small-angle X-ray scattering; poly(acrylonitrile–butadiene–styrene); mechanical properties

INTRODUCTION

Transmission electron microscopy (TEM) and small-angle X-ray scattering (SAXS) have long been used to study polymer deformation. TEM enables us to observe the deformation in a selected region and has been successfully used to study crazing in rubber-modified polymers. Early studies using the TEM technique, such as those by Bucknall,[1] Beahan et al.,[2] Kambour and Russell,[3] and Michler et al.,[4] have established the importance of multiple crazing on the toughness enhancement for the rubber-modified thermoplastics. For poly(acrylonitrile–butadiene–styrene) (ABS), it was later realized that crazing may not be the only dominant toughening mechanism.[5,6] Our own study on a high thermal resistant ABS system[7] showed the lack of craze formation in specimens that demonstrated high tensile toughness with extensive elongation and stress-whitening appearance. It was concluded that the high toughness was attributable to rubber particle cavitation and matrix shear yielding. However, evidence of the TEM work for the matrix

Correspondence to: P.-Y. B. Jar.

Contract grant sponsor: Australian Research Council.

Contract grant sponsor: Australian Synchrotron Research Program.

Contract grant sponsor: Department of Education, Training and Youth Affairs, Australia.

Journal of Applied Polymer Science, Vol. 85, 17–24 (2002)

shear yielding was limited to the matrix drawing and rubber particle deformation near the fracture surface. Shear yielding in the bulk specimen was not visible in the TEM micrographs, which was mainly because of the lack of contrast with the undeformed matrix.

SAXS, on the other hand, has been used to characterize both crazing[8] and shear yielding[9] in rubber-modified polymers. For shear yielding, the SAXS pattern reported consists of a pair of streaks in the direction of the applied stress. Although the streaks have the same orientation as the anomalous streaks observed in the craze-dominated polymers,[8] it was claimed that the anomalous streaks were not as sharp as the streaks representing the matrix shear yielding. The study in Okamoto et al.[9] reported that crazing also occurred in the polymer, but was detected only before the specimen fracture. Given that TEM was not used to examine the crazes, it was not clear whether the crazes had been initiated long before being detected by the X-ray.

TEM and SAXS were used in our previous study[10] to identify deformation mechanisms that occurred in the high thermal resistant ABS. TEM clearly showed crazes in the OsO_4-stained samples. The SAXS pattern from the shear-yielded samples had a rhomboid shape that is distinct from the pattern generated from the craze-dominated samples. The study concluded that deformation mechanisms in the fractured specimens could be positively identified by combining results from TEM and SAXS.

In addition to their use in our previous study, TEM and SAXS were used to examine a series of the high thermal resistant ABS that had been fractured under static tension and Izod impact. In this study, mechanical properties of the ABS and the associated deformation mechanisms are compared, to understand the role of the deformation mechanisms on the toughness variation of the polymer.

EXPERIMENTAL

Materials

Three high thermal resistant ABSs, ABSg1/SAN28/SMI, ABSg5/SAN28/SMI, and ABSg5/SAN22/SMI, were used in this study. As indicated by the names, the high thermal resistant ABSs are blends of ordinary ABS [ABSg1 or ABSg5, which are DENKA's (Japan) emulsion-polymerized ABS with commercial names GT-8 and GT-14, respectively], poly(styrene-*co*-acrylonitrile) (SAN28 or SAN22), and poly(styrene-*N*-phenylmale-imide) (SMI). The three high thermal resistant ABSs were carefully selected, given the limited access to the SAXS facility, to maximize the information obtained from the SAXS. As shown later under Results and Discussion, the three ABSs have the following distinctly different combinations of craze population and mechanical toughness:

- Little crazing and high toughness for ABSg1/SAN28/SMI
- Extensive crazing and medium toughness for ABSg5/SAN28/SMI
- Little crazing and low toughness for ABSg5/SAN22/SMI

We purposely chose an ABS with 40 wt % SMI, which was twice that in the commercial-grade high thermal resistant ABS, so that the specimens could be fractured in a relatively brittle manner. This avoided the possibility of extensive matrix deformation that might reduce craze visibility. It should be noted that in previous publications,[7,10] the high thermal resistant ABS contains 20 wt % SMI, which rendered a relatively high ductility.

Material information for the three high thermal resistant ABSs, such as constituent composition, rubber particle microstructure, and so forth, is given in Tables I and II. The difference between ABSg1/SAN28/SMI and ABSg5/SAN28/SMI lies among three factors for the ordinary ABS used, which are (1) molecular weight for SAN_{ABS}: 60,000 and 65,000, (2) particle size distribution: bimodal distribution of 0.1 and 0.5 μm and monodistribution of 0.3–0.5 μm, and (3) particle structure: uniform and salami-type. It is believed that the small difference in the molecular weight of SAN_{ABS}, 60,000 and 65,000, has a negligible effect on the material's mechanical properties. Therefore, the main differences between ABSg1/SAN28/SMI and ABSg5/SAN28/SMI are the size distribution and morphology of the rubber particles. Figure 1, taken from undeformed ABSg1/SAN28/SMI and ABSg5/SAN28/SMI, demonstrates the difference of the particle size and morphology between ABSg1 and ABSg5. Between ABSg5/SAN28/SMI and ABSg5/SAN22/SMI, the main difference is the acrylonitrile (AN) content of SAN_{add}, 28.9% for SAN28 and 23.6% for SAN22, as shown in Table II.

Table I ABS Used in This Study

	ABSg1/SAN28/SMI	ABSg5/SAN28/SMI	ABSg5/SAN22/SMI
Blend composition			
Ordinary ABS	ABSg1	ABSg5	ABSg5
SAN_{add}	SAN28	SAN28	SAN22
SMI	SMI55	SMI55	SMI55
Blend ratio (ABS : SAN_{add} : SMI)	40 : 20 : 40	40 : 20 : 40	40 : 20 : 40
Blend ratio in matrix (SAN_{ABS} + SAN_{add}) : SMI	1 : 1	1 : 1	1 : 1

In addition to the above-noted factors, particle distribution might be another factor that is different among the three ABSs. However, the particle distribution was found to depend on the location of the samples, and no general trend could be drawn from the TEM observation.

Overall, the three high thermal resistant ABSs have a relatively small difference in compositions, although the mechanical properties and the deformation mechanisms are very different (see Results and Discussion section below).

Mechanical Tests

Tensile and Izod impact tests were conducted to measure mechanical properties of the ABS. High thermal resistant ABS pellets were injection molded to form dumbbell-shape specimens and rectangular bars. The pellets were first dried at 100°C for 4 h and then injection-molded, with the highest resin temperature at 280°C and mold temperature 60°C. The dumbbell-shape specimens had a gauge section with constant cross section of 3×12.7 mm^2 and 65 mm length. The Izod specimens were machined from the rectangular bars with thickness of 6 mm. The rest of the dimensions followed the recommendations of ASTM D256.

An Instron universal testing machine (model 4505) was used for the tensile tests at a crosshead speed of 5 mm/min, and a conventional pendulum impact tester was used for the Izod impact tests.

TEM

The TEM examination was conducted using a transmission electron microscope (JEOL 2000 EX TEM; JEOL, Peabody, MA) operated at 200 keV. The samples were prepared from the specimens after being fractured in the static tension or the

Table II Material Information of the Constituents in the High Thermal Resistant ABS[a]

	ABSg1/SAN28/SMI	ABSg5/SAN28/SMI	ABSg5/SAN22/SMI
Ordinary ABS			
SAN_{ABS}	$SAN23_a$	$SAN23_b$	$SAN23_b$
AN content (wt %)	23	23	23
M_w of SAN_{ABS}	60,000	65,000	65,000
Bd : SAN_{ABS} (wt %)	1 : 1	1 : 1	1 : 1
Rubber particle structure	Homogeneous	Salami	Salami
Rubber particle size (μm)	0.1 and 0.5 (bimodal)	0.3–0.5	0.3–0.5
SAN_{add}			
AN content of SAN_{add} (wt %)	28.9	28.9	23.6
M_w of SAN_{add}	119,000	119,000	121,000
SMI			
Composition of SMI55 (wt%) (St : PMI : MAH)	45 : 53 : 2	45 : 53 : 2	45 : 53 : 2
M_w of SMI55	171,000	171,000	171,000

[a] There are two types of SAN23 used as SAN_{ABS}: $SAN23_a$ and $SAN23_b$. The main difference between the two is their weight-average molecular weight (M_w), 60,000 and 65,000 for $SAN23_a$ and $SAN23_b$, respectively, as shown in the table. St, styrene; PMI, phenyl-male-imide; MAH, male-anhydride; Bd, butadiene; AN, acrylonitrile.

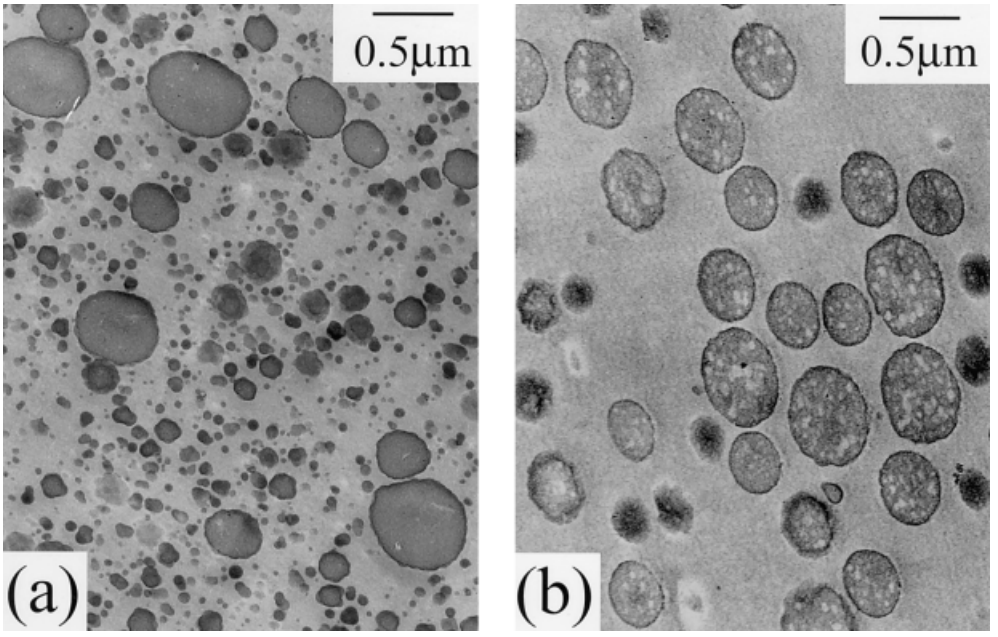

Figure 1 TEM micrographs of the high thermal resistant ABS before the mechanical tests, showing particle size distribution and structure in (a) ABSg1/SAN28/SMI and (b) ABSg5/SAN28/SMI.

Izod impact tests. The TEM examination was focused on the fracture initiation regions that were within 200 μm of the fracture surface.

The fractured specimens used to produce TEM samples were first stained in the vapor of a 2% OsO_4 solution for 2 days and then sliced using an ultramicrotome equipped with a diamond knife. A near fracture surface sectioning technique[10] was used to produce the TEM samples to examine regions immediately beneath the fracture surface.

The TEM images were first recorded in negatives (Kodak, SQ163; Kodak, Rochester, NY), and then scanned into digital files using a high-resolution negative scanner (Polaroid Sprint Scanner 45) with a resolution of 16 μm.

SAXS

The SAXS experiment was conducted at a wavelength of 1.5 Å using a tuned channel cut monochromator in BL-20B (Photon Factory, Tsukuba, Japan). The distance from the specimen to the imaging plate (IP) was 1783 mm. Details of the setup were previously described.[10] All SAXS patterns presented in this study were obtained with an exposure duration of 30 s.

SAXS samples were strips (0.5 mm thick, 3.3 mm wide) that were sliced from the tested specimens across the thickness and along the specimen length direction using a slow cutter (Leco VC-50). To highlight the contour shape of the diffraction pattern, the SAXS patterns presented in this study were converted from the original patterns using the Posterize command (8 levels) that is available in Adobe Photoshop version 5 (Adobe, San Jose, CA).

RESULTS AND DISCUSSION

The mechanical properties for the three high thermal resistant ABSs are summarized in Table III. All values in Table III follow the trend in the order of ABSg1/SAN28/SMI > ABSg5/SAN28/SMI > SANg5/SAN22/SMI. The ABSg1/SAN28/SMI showed much higher toughness than that of the other two ABSs, in both static tension and Izod impact.

The TEM micrographs are summarized in Figure 2, in which crazes are visible in all micrographs, although the craze density varies. Figure 2(a), taken from ABSg1/SAN28/SMI under static tension, contains a very small number of crazes. The number of crazes increases in Figure 2(d), taken from the same material but tested under the Izod impact. Both Figure 2(a) and (d) show

Table III Mechanical Test Results of the ABS Used in the Study

	ABSg1/SAN28/SMI	ABSg5/SAN28/SMI	ABSg5/SAN22/SMI
Tensile test			
Maximum strength (MPa)	47	42	34
Maximum elongation (mm)	3.84	2.82	2.06
Total fracture energy (J)	4.84	2.68	1.70
Izod impact toughness (J/m)	39.2	28.4	24.5

rubber particle cavitation in large and small particles, and the cavitated particles appear in clusters. It should be noted that the percentage of the cavitated particles does not appear to be as high as that reported previously.[12] This was possibly because of the brittle nature of the specimens used here, which reduced the amount of deformation before the fracture.

For ABSg5/SAN28/SMI, as shown in Figure 2(b) and (e), the crazes are clearly visible in both static tension and Izod impact specimens, and the number of crazes generated from each particle is

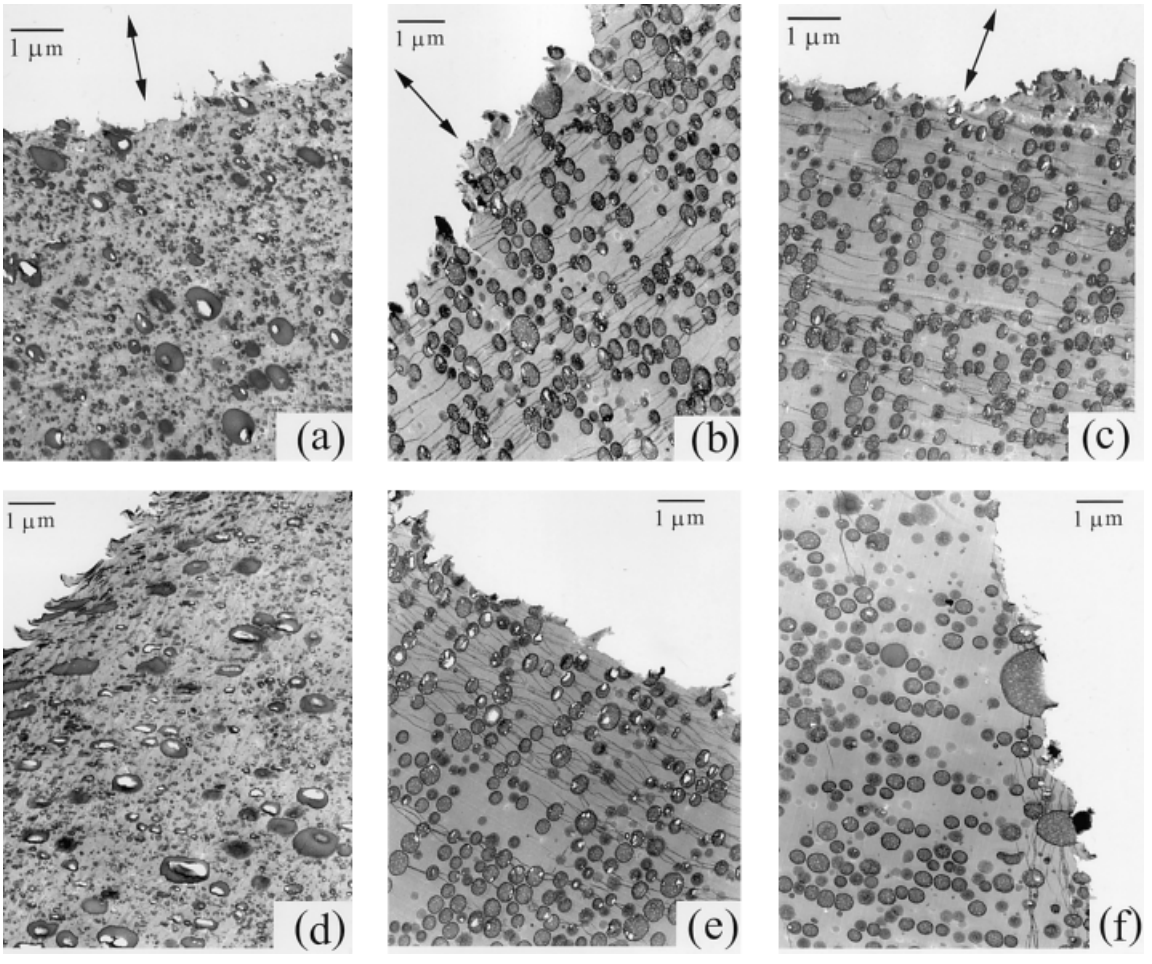

Figure 2 TEM micrographs in the area beneath the fracture surfaces: (a) static tension, ABSg1/SAN28/SMI55; (b) static tension, ABSg5/SAN28/SMI55; (c) static tension, ABSg5/SAN22/SMI; (d) Izod impact, ABSg1/SAN28/SMI; (e) Izod impact, ABSg5/SAN28/SMI55; (f) Izod impact, ABSg5/SAN22/SMI55. The arrows in (a), (b), and (c) indicate the direction of the applied stress.

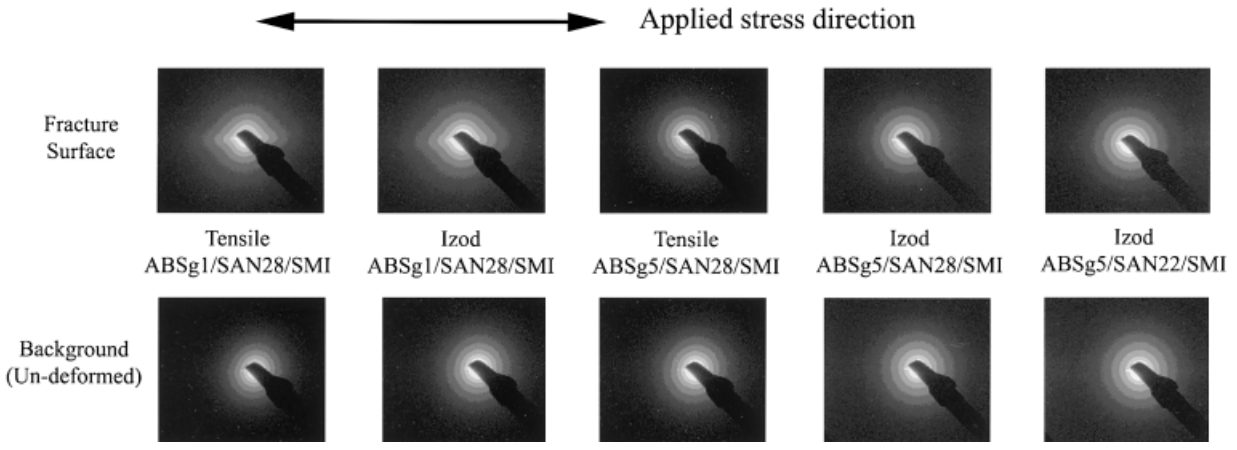

Figure 3 SAXS pattern of the specimens used in the study. The applied stress is in the horizontal direction.

larger than that in ABSg1/SAN28/SMI. Cavitation also occurred in some particles in Figure 2(b) and (e), although the extent of particle cavitation is less than that shown in Figure 2(a) and (d), possibly because of the ABSs' relatively low ductility, as shown in Table III.

The TEM micrograph from the static tension fractured specimen of ABSg5/SAN22/SMI [Fig. 2(c)] bears some similarity to that of Figure 2(b), except that the craze growth in Figure 2(c) is less extensive. On the other hand, the TEM micrograph from the Izod impact specimen of ABSg5/SAN22/SMI [Fig. 2(f)] showed very few crazes, which mainly appear in regions that are very close to the fracture surface.

SAXS patterns for the three ABSs are summarized in Figure 3, in which the SAXS pattern from the static tension of ABSg5/SAN22/SMI is omitted because of its similarity to that from the static tension of ABSg5/SAN28/SMI. The upper patterns in Figure 3 were obtained from regions within 0.2 mm of the fracture surface, whereas the lower patterns were obtained from the undeformed regions for comparison. As expected, the SAXS patterns for the undeformed regions are circular. So are those from the deformed regions of the specimens that contain ABSg5. On the other hand, both static tension and Izod impact specimens of ABSg1/SAN28/SMI generated lemon-shape SAXS patterns with the orientation in the direction of the applied stress. Given that the lemon-shape SAXS pattern is an indication of shear yielding, the results suggest that shear yielding had occurred in ABSg1/SAN28/SMI under both static tension and Izod impact, but not in the two high thermal resistant ABSs containing ABSg5.

Because shear yielding did not occur in the ABS containing ABSg5, crazing should be the only matrix deformation mechanism in these materials. Despite the dramatic difference in craze population between Figure 2(e) and Figure 2(f), from ABSg5/SAN28/SMI and ABSg5/SAN22/SMI, respectively, their Izod impact toughness values were not appreciably different, suggesting that the craze population affected their Izod impact toughness only slightly.

It has long been established that the craze population is directly linked to the fracture toughness for rubber-modified polymers such as ABS and high-impact polystyrene (HIPS). However, the results from ABSg5/SAN28/SMI and ABSg5/SAN22/SMI suggest that the significant increase in craze population (the former of which was threefold that of the latter, judging from the TEM micrographs in Fig. 2) does not warrant the equivalent significance for the toughness increase (only $\sim$ 15%). The two ABSs show a scanty degree of toughness compared with the toughness of ABSg1/SAN28/SMI, which has shear yielding involved in the matrix deformation. Therefore, we believe that crazing exerts a lesser effect than that of shear yielding on the toughness enhancement.

Given that crazing was not the dominant deformation mechanism for ABSg1/SAN28/SMI, the widely accepted toughening mechanism of using the bimodal particle size distribution to stop the craze growth does not provide a satisfactory explanation for the superior toughness of ABSg1/SAN28/SMI. Besides, the particle size difference in ABSg1 is probably too small to benefit the toughness, judging from the optimum bimodal particle size distribution previously reported.[9]

The results also suggest that shear yielding can coexist with crazing in the ABS. By combining results from TEM and SAXS, we were then able to identify all possible deformation mechanisms in the material. This conclusion is consistent with that reported previously,[10] and the results suggest that shear yielding is a main attribute to the superior toughness of the ABS.

A controversy exists on the sequential occurrence of shear yielding and crazing. Gilbert and Donald[13] suggested that for HIPS the formation of thin bridges between the crazes promotes the occurrence of shear yielding. Therefore, crazing should have occurred before shear yielding. Based on the *in situ* SAXS study of HIPS, Okamoto et al.[9] suggested that the shear yielding occurred before the crazing. Crazing was detected only shortly before the sample fracture. Our results show that shear yielding was the dominant deformation mechanism for ABSg1/SAN28/SMI under static tension, which contained very few crazes in the matrix. On the other hand, ABSg5/SAN28/SMI and ABSg5/SAN22/SMI showed extensive crazing with no trace of shear yielding. Therefore, we believe that for the ABSs studied, shear yielding and crazing do not necessarily occur in sequence. They are probably two independent deformation events of which the occurrence depends on the composition of the ABSs.

We speculate that the particle morphology is the main factor that determines whether shear yielding or crazing dominates the deformation in the three ABSs, resulting in different mechanical properties. Using the finite-element method,[14] we have shown that when the Poisson's ratio of the rubber particle is close to 0.5, the residual thermal stress, attributed to the mismatch of thermal expansion coefficients between the rubber particle and the matrix during cooling, can be significant enough to alter the normal stress distribution in the matrix surrounding the rubber particle. For the ABS containing the rubber particles of uniform structure, Poisson's ratio is expected to be very close to 0.5; however, for the ABS with the salami-type rubber particles, the existence of polystyrene inclusions reduces the Poisson's ratio of the particle, thus reducing the thermal stress and its effect on the normal stress distribution in the matrix. Under the assumption that the three ABSs used in the study were processed under the same conditions (thus the same temperature profile for the cooling), the thermal stress in ABSg5/SAN28/SMI is expected to be lower than that in the ABSg1/SAN28/SMI. Therefore, the thermal stress of the latter is expected to have a stronger effect on the normal stress suppression than that of the former. Further study is planned to provide the supporting evidence for the above speculation.

CONCLUSIONS

The mechanical properties for the high thermal resistant ABS under static tension and Izod impact and the associated deformation mechanisms were investigated. The study supports our previous conclusion that crazing and shear yielding can be identified using TEM and SAXS, respectively. Shear yielding was found to occur in both static tension and Izod impact specimens of ABSg1/SAN28/SMI, which also showed the highest toughness. Deformation in the other two ABSs was dominated by crazing, and the toughness variation was found to be relatively insensitive to the craze population. The study also showed that shear yielding and crazing can coexist, although their occurrence is not necessarily sequential.

The study showed that the TEM alone is insufficient to identify all deformation mechanisms in the ABS, and that the multiple crazing is not as effective as the shear yielding for the toughness enhancement. We also speculated that rubber particle morphology has caused the variation of the deformation mechanisms, and the evidence for the speculation is currently being examined.

Financial support for the work was from Australian Research Council and the Australian Synchrotron Research Program under the Major National Research Facilities program. Part of the travel support for the SAXS work also came from Targeted Institutional Links program (administered by Department of Education, Training and Youth Affairs, Australia). The authors also acknowledge the assistance from J. Hester and G. Foran of the Australian National Beamline Facility; R. Lee and S. Stowe of the Australian National University; T. Kuboki of Kyushu University; and P. M. O'Neill of the Australian Defense Force Academy, who contributed to the experimental work.

REFERENCES

1. Bucknall, C. B. Toughened Plastics; Applied Science: London, 1977.
2. Beahan, P.; Thomas, A.; Bevis, M. J. J Mater Sci 1976, 11, 1207.
3. Kambour, R. P.; Russell, R. R. Polymer 1970, 12, 237.

4. Michler, G.; Gruber, K.; Pohl, G.; Kaestner, G. Plast Kaut 1973, 20, 756.
5. Breuer, H.; Haff, F.; Stabenow, J. J Macromol Sci Phys 1977, B14, 387.
6. Donald, A.; Kramer, E. J. J Mater Sci 1982, 17, 1765.
7. Jar, P.-Y. B.; Wu, R. Y.; Kuboki, T.; Takahashi, K.; Shinmura, T. J Appl Polym Sci 1999, 71, 1543.
8. Brown, H. R.; Kramer, E. J. J Macromol Sci Phys 1981, B19, 487.
9. Okamoto, Y.; Miyagi, H.; Uno, T.; Amemiya, Y. Polym Eng Sci 1993, 33, 1606.
10. Jar, P.-Y. B.; Lee, R.; Creagh, D. C.; Konishi, K.; Shinmura, T. J Appl Polym Sci 2001, 81, 1316.
11. Jar, P.-Y. B.; Wu, R. Y.; Kuboki, T.; Takahashi, K.; Shinmura, T. J Mater Sci Lett 1997, 16, 1489.
12. Jar, P.-Y. B.; Shinmura, T.; Konishi, K. J Mater Sci Lett 2000, 19, 73.
13. Gilbert, D. G.; Donald, A. M. J Mater Sci 1986, 21, 1819.
14. Jar, P.-Y. B.; Todo, M.; Takahashi, K.; Konishi, K.; Shinmura, T. Plast Rubber Compos Process Appl 2001, 30, 101.